Jestr

Journal of Engineering Science and Technology Review 17 (4) (2024) 109-118

Research Article

JOURNAL OF
Engineering Science and Technology Review

www.jestr.org

Rock Breakability Assessment and the Impact of the Produced Aggregate on the Elastic Modulus of Concrete

Kunlong Zhao[1], Wengui Jia[2], Xiang Ma[3,*], Xiao Liu[3] and Wenbo Wu[1]

[1]*Powerchina Northwest Engineering Corporation Limited, Xi'an, 710065, China*
[2]*Huaneng Gansu Energy Development Corporation Limited, Gansu,730000, China*
[3]*Xi'an Thermal Power Research Institute Corporation Limited, Xi'an, 710032, China*

Received 19 May 2024; Accepted 28 July 2024

Abstract

In engineering construction, rocks broken by mining and tunnel excavation are often used as concrete aggregates, and rock fragmentation influences the elastic modulus of concrete. To improve the efficiency of rock breaking and the application effects of rock aggregates, this work proposed a method for evaluating rock breakability and the impact of the produced aggregate on the elastic modulus of concrete. The breakability of rock and its impact on concrete performance were studied based on fractal theory. A physical parameter characterization method was proposed to quickly compare the difficulty of rock fragmentation, characterizing the breakability of rocks and the processability of aggregates. The relationship between the relative specific surface area of aggregates and their main physical properties was established. The influence of rock breakability on the elastic modulus of concrete was analyzed through laboratory tests of uniaxial compression on concrete. Results demonstrate that the content of firm components in the rock mineral composition is significant, and the particle content of the main mineral components is positively correlated with the relative specific surface area of the fragmented aggregates. The relative specific surface area of the aggregates is negatively correlated with the fineness modulus and apparent density of the aggregates and positively correlated with the stone powder content and crushing index. The relative specific surface area of the aggregates shows a linear decreasing relationship with the water-to-binder ratio and elastic modulus. For C30 (C40) concrete, the water-to-binder ratio increased by 19.4% (21.4%), and the static compressive elastic modulus increased by 22.5% (25.0%). This study provides a particular guiding significance for the rapid and effective breaking of rock bodies and the resource utilization of aggregates.

Keywords: Rock, Breakability, Aggregate, Concrete, Elastic Modulus

1. Introduction

Mining and tunnel excavation have become indispensable parts of economic construction. However, mining and tunnel excavation face the challenge of achieving rapid and effective rock breaking and resource utilization. Conducting a study on rock breakability evaluation is critical to achieving rapid and effective rock breaking. Moreover, as one of the essential raw materials for concrete engineering, crushed rock aggregate significantly impacts the mechanical properties of concrete, making the selection of material sources significant. The premise for preparing high-quality concrete materials is to obtain the basic properties of aggregates quickly, compare the differences between different aggregates, and ultimately select the appropriate material sources. Therefore, studying rock breakability evaluation and the impact of the produced aggregate on the elastic modulus of concrete is a requirement for safe, efficient, and green resource development, and it has excellent engineering significance.

Predicting and assessing the risk of rock fragmentation are crucial. Scholars have explored the impact of stress conditions and rock-cutting rates on hard rock fragmentation [1, 2] and have used a combination of finite element modeling and image processing to identify rock fragmentation sizes and establish average fragment prediction models [3-6]. They found that the presence of pre-existing fractures is crucial for fragmentation, and these findings have been used to optimize the size of rock fragments and to design the tool spacing for double-disc cutters in tunnel engineering [7, 8]. In addition, scholars have further studied the impact of rock-made aggregates on the elastic modulus of concrete, proposing a new meshing method to discretize mesoscale models of concrete with arbitrary interface transition zone thicknesses to explore the influence of mesostructure characteristics on the elastic modulus of concrete [9] and researching different chemical modification methods to improve the elastic modulus of recycled concrete aggregate (RCA) [10]. However, no effective physical parameter has been proposed to compare the ease of rock fragmentation, which is not conducive to achieving rapid and effective rock breaking. Studies on the impact of rock-made aggregates on the elastic modulus of concrete are still minimal. Therefore, conducting rock breakability evaluation and analyzing its impact on the elastic modulus of concrete, providing technical support for preparing high-quality concrete materials, are urgently needed to better apply crushed rock in practical engineering.
This study proposed a physical parameter, namely, relative specific surface area, based on the fractal dimension method to quickly compare the ease of rock fragmentation, characterizing the breakability of rocks and the processability of aggregates. The aim is to establish the relationship between the relative specific surface area of aggregates and their main physical properties, reveal the

*E-mail address: 1528138103@qq.com
ISSN: 1791-2377
doi:10.25103/jestr.174.13

impact of rock breakability on the performance of concrete elastic modulus, and provide a reference for achieving rapid and effective rock breaking and resource utilization of aggregates.

2. State of the art

Rock breakability evaluation is critical to achieving rapid and effective rock breaking and resource utilization [11-14]. In recent years, scholars have conducted extensive research, mainly focusing on rock fragmentation identification and impact parameter studies, as well as rock fragmentation modeling and prediction.

In terms of rock fragmentation identification and impact parameter studies, Räisänen [15] investigated the relationship between the petrology and mechanical properties of the hybrid subvolcanic Jaala–Iitti complex in southeastern Finland, using polarizing microscopy to quantify the petrology of polished thin sections to determine their modal composition and grain size distribution, and to measure their anti-breakability and wear resistance. Findings show that the type and size distribution of minerals have a significant impact on the abrasion rate and mechanical properties of aggregates. Azadmehr et al. [13] argued that identifying and determining the impact parameters are crucial to assessing rock mass breakability. They proposed a method that comprehensively considered the direct and indirect impacts of impact parameters on rock mass breakability using the classical Rock Engineering System (RES) and the Matrix Impact Cross Multiplication Classification method. Zou et al. [2] designed a new triaxial test device for indentation testing to explore the impact of stress conditions and rock cutting rates on hard rock fragmentation, studying the pore size and fragmentation efficiency of granite by analyzing the variation patterns of thrust, penetration depth, debris characteristics, and failure modes. Wang and Tonon [16] used discrete element programs to simulate rock fragmentation caused by impacts in rockfall analysis, finding that impact velocity, angle of incidence, pre-existing fractures, and ground stiffness all significantly influence impact fragmentation. The results indicated that impact fragmentation occurred only locally in the impact area for homogeneous blocks and did not produce large fragments. Large fragments were produced only when open fractures in the rock mass or completely persistent closed fractures were present. Elevli et al. [17] used stepwise multiple linear regression analysis to determine the dominant degree of each impact parameter on fragmentation and established a fragmentation prediction model. The results showed that rock mass properties, material width, and specific charging were fragmentation's main parameters. Tosun [18] established correlations between blast surface discontinuity characteristics and rock strength to predict drill bit penetration rates and between specific charging coefficient and drill bit penetration rates to predict muck pile fragmentation, conducting blasting tests in two limestone quarries. These studies suggested that the fragmentation of rock under compression depended on the rock's self-sustaining failure and the available energy at peak strength. However, no studies have attempted to correlate rock brittleness with its corresponding compressive fragmentation. The failure of rock under conventional compression testing and the subsequent fragment size distribution are poorly understood phenomena. According to the ISRM (2007) recommended method [19], a closed-loop servo-controlled testing machine was used to determine the post-peak moduli of various rocks and to conduct brittle compressive fragmentation. Various brittle concepts were evaluated based on static mechanical properties, energy balance, normalized pre-failure curves, and extended strain criteria. On the basis of a comparison with the fragment sizes obtained from compression, the brittle concepts of static mechanical properties suggest that a high value corresponds to fine fragmentation. The concepts of normalized pre-failure curves and extended strain criteria seem to treat the fragmentation of Types I and II rocks as a single entity, showing a better correlation with the fragmentation degree of separated samples than other concepts. These concepts are related to the post-peak moduli of rocks and can be employed to quantify rock brittleness under compression [20]. In the area of rock fragmentation modeling and prediction, Kucewicz et al. [5] proposed a reliable and simplified method for modeling rock fragmentation, discovering that the presence of pre-existing fractures was crucial for fragmentation, especially when drilling took place near a free rock face. Ni et al. [21] conducted a series of theoretical analyses and numerical simulations to study the dynamic fragmentation effects of cyclic blasting on deeply buried rock masses under different ground stress conditions. The results indicated that rock blast fractures extended along the direction of the maximum principal stress, and the number of newly fragmented rock elements gradually decreased with continuous single-hole blasting. Sharma et al. [6] collected blasting design, rock mass, and debris data from 100 explosive coal seam explosions in a coal mine. They used soft computing techniques to establish an average fragment size prediction model, determining the maximum variable affecting average fragment size and its optimal value in high-temperature coal seam blasting. Li et al. [3] developed a combination of finite element modeling and image processing to study rock fracturing caused by decoupled charging blasting, simulating the rock fracturing caused by decoupled charging blasting with different decoupling ratios, coupling media, and decoupled charging patterns. The simulated fracture network was obtained by eliminating the damaged elements whose damage level exceeded the crack formation threshold. Hosseini et al. [1] used data collected from 64 blasts at the Zarshoran gold mine in Iran to predict and assess the risk of rock fragmentation, establishing a new RES. While these studies, to some extent, replicated the rock fragmentation process through numerical simulation and provided technical support for the prediction and assessment of rock fragmentation, they did not reveal the fragmentation characteristics of the original rock at the micro and fine scales nor did they explore the impact of mineral particle composition on rock breakability. Existing studies have not proposed effective physical parameters to compare the ease of rock fragmentation, which has caused difficulties in rapidly and effectively breaking rock bodies.

Regarding the impact of rock-made aggregates on the elastic modulus of concrete, Chen and Xiao [9] proposed a new meshing method to discretize mesoscale models of concrete with arbitrary interface transition zone (ITZ) thicknesses, and the established numerical model could accurately estimate the elastic modulus of concrete while also discussing the impact of mesostructure characteristics on the elastic modulus of concrete. The results showed that the aggregate shape has a minimal effect on the elastic modulus of concrete, and the ITZ's thickness has less influence than the volume fraction of the aggregate and

mortar. In addition, the elastic modulus of concrete predicted by randomly configured three-dimensional numerical models showed negligible dispersion. Liang et al. [10] studied three chemical modification methods to improve the elastic modulus of RCA, namely, fly ash-silica fume slurry, nano-SiO2 solution, and carbonation modification. The results indicated that the different modification methods had similar impacts on the elastic modulus of RAC as they did on the corresponding peak stress, consistent with the effects on the quality of the recycled aggregate. The modified RAC had fewer micropores, and the ITZ and hydration products were denser, which was the main reason for the increased elastic modulus. The above studies mainly studied the impact of mineral categories and the size and distribution of mineral particle sizes on the abrasion rate and mechanical properties of aggregates and proposed numerical simulation methods for simulating rock fragmentation. However, studies on the impact of rock-made aggregates on the elastic modulus of concrete are still limited.

The achievements mentioned above mainly focus on identifying rock fragmentation, impact parameters, modeling, breakability prediction, and the impact of rock-made aggregates on the elastic modulus of concrete. However, studies have not proposed effective physical parameters to compare the ease of rock fragmentation, which is not conducive to guiding the rapid and effective breaking of rock bodies. Instead, existing work on the impact of rock-made aggregates on the elastic modulus of concrete is primarily concentrated on numerical simulation, and practical engineering applications have not been verified. Therefore, this study proposes using fractal dimensions to establish a physical parameter for quickly comparing the ease of rock fragmentation to characterize rock breakability and the processability of aggregates and to establish the relationship between the relative specific surface area of aggregates and their main physical properties. Through original rock micro testing, original rock breakability tests, and uniaxial compression tests of concrete with the same design grade, this study reveals the impact of significant mineral components on rock breakability. Moreover, it analyzes the performance impact of rock breakability on the elastic modulus of concrete.

The remainder of this study is organized as follows. Section 3 describes the micro characteristics of the original rock and designs original rock breakability tests and concrete mechanical performance tests. Section 4 establishes the relationship between the relative specific surface area of aggregates and their main physical properties, prepares concrete with the same design grade for uniaxial compression tests, and analyzes the impact of rock breakability on the performance of concrete. The final section summarizes the study and presents the relevant conclusions.

3. Methodology

3.1 Microscopic Characteristics of the Original Rock

Rocks are solid aggregates with a stable shape composed of one or more minerals and natural glass. The types and proportions of mineral compositions vary for different types of rocks, and the range of mineral grain sizes is also different, leading to variations in their macroscopic mechanical properties. Granites, tuffs, diorites, and sandstones from the Tibet and Xinjiang regions were selected as representative samples for microscopic analysis and research. Thin-section tests were conducted on these samples, and the primary mineral compositions and structures of each rock were analyzed using a scanning electron microscope, with the following results: The composition of granite rock mainly includes quartz, plagioclase, potassium feldspar, biotite, and other metallic minerals. Potassium feldspar, plagioclase, and quartz account for more than 90% of the content, with potassium feldspar and plagioclase crystals being relatively coarse, quartz having undergone fragmentation and recrystallization to form an aggregate of embedded granular particles, and biotite mainly distributed between quartz and feldspar grains, with other metallic minerals and biotite coexisting. The composition of tuff mainly includes plagioclase spherulites, altered fine volcanic ash, quartz rock fragments, volcanic breccia, and other altered minerals. The spherulites in the rock come from the volcanic cap, mainly containing quartz and albite. The content is above 70%, both having angular morphologies, with a significant difference in grain size. The altered fine volcanic ash shows idolization, mainly distributed between volcanic debris, with volcanic breccia mainly composed of trachyte and granite and other altered minerals and altered volcanic ash filling between the spherulites and breccia. The composition of diorite mainly includes altered plagioclase, amphibole, quartz, and other altered minerals. The content of altered plagioclase is 45%, with a strong sericitization, and after alteration, only the original directional morphology of the plagioclase remains, with the original mineral structure disappearing. Amphibole and quartz account for about 30% and 20%, respectively, both showing a macroscopic directional arrangement with the characteristics of tectonic dynamic action, and the altered mineral is mainly sericite replacing plagioclase. The composition of sandstone mainly includes fragmented feldspar, fragmented quartz, biotite, and carbonate. The content of fragmented feldspar and fragmented quartz is about 80%, belonging to a fine aggregate, and cannot be measured accurately; it usually measures below 0.01 mm. This result is due to the strong dynamic action that has changed the composition and structural texture of the original rock. Most minerals in the original rock have been fragmented and recrystallized under dynamic action, with only some quartz remaining in a residual form. Biotite and carbonate form mainly due to thermal metamorphism and hydrothermal alteration, causing the biotite in the rock to exhibit most of it in an undirected arrangement and some in a directed arrangement, with the rock also showing carbonatization in some areas.

For the sake of describing the size distribution of rock mineral particles, they are classified into four grain size ranges according to the maximum size of the mineral particles' planar projection: microscopic (<0.2 mm), fine (0.2 mm–2 mm), medium (2 mm–5 mm), and coarse (>5 mm). See Table 1 for details.

Table 1. Main Mineral Compositions and Their Proportions in Different Rocks

Rock type	Main mineral component	Mineral size range proportion (mm)			
		<0.2 Particulate	0.2–2 Fine particle	2–5 Medium grain	>5 Coarse fraction
Granite	Feldspar	5	42	18	
	Quartz	10	16		

	Biotite		6		
	Others	3			
Tuff	Feldspar	25	25		
	Quartz	21			
	Cinerite	19			
	Volcanic breccia			7	2
	Others	1			
Diorite	Feldspar	10	35		
	Hornblende		33		
	Quartz	14	6		
	Others	2			
Sandstone	Feldspar	56			
	Quartz	23			
	Biotite	11			
	Carbonate	8	2		

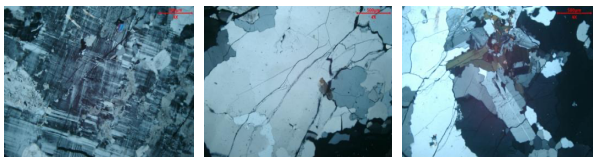

(a) Potash Feldspar (b) Quartz (c) Feldspar and Biotite

Fig. 1 Microstructure of Granite (500× magnification)

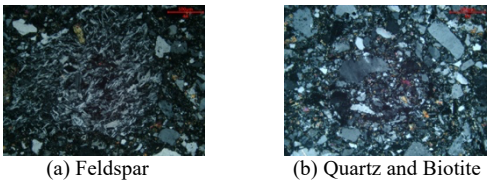

(a) Feldspar (b) Quartz and Biotite

Fig. 2 Microstructure of Tuff (500× magnification)

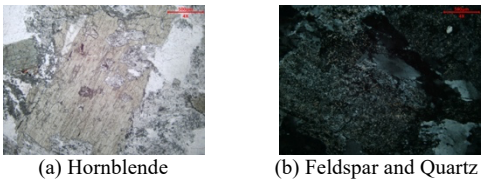

(a) Hornblende (b) Feldspar and Quartz

Fig. 3 Microstructure of Diorite (500× magnification)

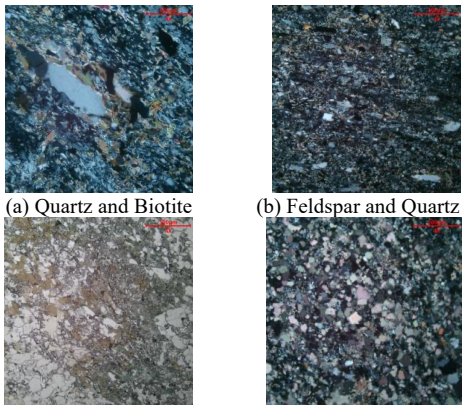

(a) Quartz and Biotite (b) Feldspar and Quartz

(c) Biotite (d) Carbonate

Fig. 4 Microstructure of Sandstone (500× magnification)

Table 1 and Figs. 1 to 4 show that the main mineral components in the four types of rocks are feldspar and quartz minerals, with their content exceeding 60%, which are the main mineral components that influence the properties of the rocks. The mineral grains in granite are mainly composed of fine, medium, and microscopic particles, while those in tuff are primarily composed of fine, microscopic, medium, and coarse particles. Diorite and sandstone are mainly composed of fine and microscopic particles. Among them, the content of microscopic particles in granite is the least, followed by diorite, then tuff, and the content of microscopic particles in sandstone is the highest. Muscovite generally has a lamellar structure and low hardness, which is considered disadvantageous for strength, especially when the mineral grain size is large. In this test, the content of muscovite in sandstone is the highest, followed by granite, and no muscovite is present in diorite and diorite.

3.2 Original Rock Breakability Test

The breakability of a rock refers to the ease or difficulty of breaking the rock from large pieces into small pieces, which can be understood as the ease of rock fragmentation. It reflects the rock's resistance to external force fragmentation and is one of the physical and mechanical properties of the rock. The hardness of the rock is well known to be positively correlated with the strength of the aggregates produced but negatively correlated with the rock's breakability. In engineering, when selecting the source of materials, choosing rocks with better breakability as the aggregate for concrete is advisable as long as they meet the design requirements. Such rocks will significantly reduce the wear and tear costs of the equipment and speed up the production progress of the aggregate. After being subjected to external forces such as blasting mining and mechanical crushing, rocks will form artificial aggregates with altered shapes and sizes, and they will also have a certain degree of randomness and irregularity. Therefore, they can be studied using fractal theory [13,14]. The concept of the relative specific surface area of the artificial aggregate is introduced to characterize the degree of fragmentation of the aggregate. A large specific surface area corresponds to a high breakability of the rock. The specific surface area of the aggregate can be calculated by considering the aggregate particle size distribution, the fractal gradation of the aggregate, and the fractal body of the aggregate (as shown in Eq. 1). This provides a theoretical basis for comparing the breakability of different rocks. The specific surface area of the aggregate is calculated using Eqs. 2 to 7.

$$P(x)=\frac{x^{-(D-3)}-x_{\min}^{-(D-3)}}{x_{\max}^{-(D-3)}-x_{\min}^{-(D-3)}}\times 100\% \tag{1}$$

where $P(x)$ is the passing rate of the aggregate through the sieve; $x_{\max}$ is the maximum sieve size; $x_{\min}$ is the minimum sieve size; and D is the fractal dimension of the aggregate gradation.

$$S=\frac{k_s}{k_v}\times\frac{\delta_{\min}^{2-D}}{\rho}\times\frac{x_{\max}^{D_s-D}-x_{\min}^{D_s-D}}{x_{\max}^{3-D}-x_{\min}^{3-D}} \tag{2}$$

$$V_0^x=k_v x^3 \tag{3}$$

$$A_0^x=k_s x^2 \tag{4}$$

$$x = \sqrt[3]{\frac{6V_0^x}{\pi}} \tag{5}$$

$$\frac{k_s}{k_v} = \frac{A_0^x \times x}{V_0^x} = (6/\pi)^{1/3} \times A_0^x \times V_0^{x(-2/3)} \tag{6}$$

where S is the specific surface area of the aggregate; ρ is the apparent density of the aggregate; D_s is the surface fractal dimension of the aggregate; δ_{min} is the minimum scale length used to measure the fractal area of the aggregate; k_s, k_v are the surface shape factor of the aggregate and the volume factor of the aggregate, respectively; x is the equivalent particle size of the aggregate (calculated according to the principle of equal volume); V_0^x is the surface area of the aggregate with an equivalent particle size x; and A_0^x is the volume of the aggregate with an equivalent particle size x. For convenience of calculation, the following assumptions are made: (1) The aggregate surface is smooth, and γ is taken as 2; (2) The aggregate particle shape is spherical, i.e., $k_s/k_v = 6$; (3) The minimum particle size of the aggregate is the minimum scale used to measure the fractal of the aggregate, i.e., $\delta_{min} = x_{min}$. The specific surface area of the aggregate can be obtained using Eq. 2.

The fractal dimension D of the aggregate has a certain functional relationship with the particle size distribution of the aggregate. The specific surface area of the aggregate is related to the fractal dimension D and the particle shape, as well as the particle size distribution of the aggregate. Through the rock fragmentation tests, the specific surface area of the aggregate is simplified to the following formula:

$$S_r = k(i)\sum \frac{\mu(i)}{\gamma(i)} \tag{7}$$

where $k(i)$ is a constant that depends on the aggregate crushing and processing equipment; $\mu(i)$ is the mass ratio of each grade of material; and $\gamma(i)$ is the equivalent particle size of each grade of material, which the average particle size can replace. The value of k can be determined by plotting a curve of the aggregate-specific surface area against aggregate gradation from multiple tests. The slope of the curve is equal to $k(i)$. However, for convenience of comparison, $k(i)$ is usually taken as 10. In this way, Eq. 7 is simplified to a simpler calculation formula, referred to as the relative specific surface area.

3.3 Concrete Mechanical Property Test

3.3.1 Raw Materials

The cement used is P·O 42.5 cement produced by Gaozheng Lhasa Cement Plant, the fly ash is F-class II fly ash produced by Weih River Power Generation Co., Ltd., and the water-reducing agent is 405 powder-type polycarboxylate high-performance water-reducing agent produced by Shanxi Kaidi Additive Factory, with an optimal dosage of 0.18%, a water reduction rate of 28.6%, and Gk-9A air entraining agent. The original rock is crushed using a PE 250 × 400 jaw crusher and a PCΦ400 × 300 hammer crusher (Fig. 5), and the crushed aggregate is sieved into medium stone, small stone, and artificial sand. The particle gradation of the artificial sand is tested, and the gradation is adjusted by removing stone powder and particles larger than 2.5 mm to make them roughly equivalent. The crushing index of the coarse aggregate is then tested.

Fig. 5 PCΦ400 × 300 Hammer Crusher

3.3.2 Mix Proportion

This test selected grade II standard concrete with strength grades of C30 and C40. The design curing period is 28 days, the slump at the machine outlet is controlled between 70 and 90 mm, and the air content is approximately 4.5%. The fly ash content is 20%, and the water-reducing agent content is selected at the optimal dosage. The air-entraining agent content is controlled to meet the air content requirements, and the water and sand ratio is determined through trial mixing, with the best performance of the mixture as the criterion.

3.3.3 Compressive Strength and Static Compressive Elastic Modulus

The specimen dimensions are 150 mm × 150 mm × 150 mm for cubic concrete specimens and φ 150 mm × 300 mm for circular concrete specimens for axial compressive and static compressive elastic modulus testing. The specimens are placed in a curing room for 24 hours before being demolded and moved into the standard curing room. Mechanical tests are conducted when the concrete reaches a curing age of 28 days. The cubic compressive strength of concrete, the axial compressive strength, and the axial compressive strength are calculated according to Eqs. 8, 9, and 10, respectively.

$$f_{cc} = \frac{F}{A} \tag{8}$$

$$f_c = \frac{F}{A} \tag{9}$$

$$E_c = \frac{F_2 - F_1}{A} \times \frac{L}{\Delta L} \tag{10}$$

where f_{cc} is the compressive strength, MPa; f_c is the axial compressive strength, MPa; E_c is the static compressive elastic modulus, MPa; F is the maximum failure load, N; F_2 is the 40% limit failure load, N; F_1 is the load at 0.5 MPa stress, N; A is the bearing area of the specimen, mm^2; L is the measuring span of the deformation, mm; and ΔL is the average value of the specimen deformation from 0.5 MPa stress to 40% failure stress, mm.

4. Result Analysis and Discussion

4.1 Original Rock Breakability Test

The gradation distribution and relative specific surface area of the broken aggregate at each level are shown in Table 2.

Table 2. Grain Composition and Relative Specific Surface Area of Aggregate After Crushing

Serial number	Size of the original rock (mm)	Distribution of particle gradation of aggregates at all levels (%)				Relative specific surface area S_r
		(40–80) mm	(20–40) mm	(5–20) mm	<5 mm	
H-JP	80–150	15.6	33.7	37.9	12.8	73.23
N-JP	80–150	30.4	40.7	19.3	9.6	57.10
SC-JP	80–150	22.4	36.7	30.3	10.6	64.43
SH-JP	80–150	28.3	45.2	18.4	8.1	53.65

The test results show that the relative specific surface area of crushed granite is the largest, followed by diorite, then tuff, and finally sandstone, which has the smallest relative specific surface area. This finding indicates that granite is the most easily broken among the four types of rocks, while sandstone is the most difficult to break.

4.1.1 Influence of Main Mineral Component Content on Rock Breakability

Comparative analysis reveals that all four rocks contain quartz and feldspar as their main mineral components. Therefore, the focus is the influence of quartz and feldspar content on rock breakability. The results are shown in Fig. 6. The test results show that, except for granite, as the quartz content increases in the four types of rocks, the relative specific surface area of the rock gradually decreases. The same trend is observed with the feldspar content, with the total content of feldspar and quartz minerals being higher, resulting in a smaller specific surface area, indicating that the rock is more challenging to break. This finding further verifies the conclusion that the rock's content of hard components is negatively correlated with the rock's breakability. However, granite exhibits an anomaly, not showing a negative correlation pattern with increased quartz and feldspar content. This phenomenon could be due to the presence of biotite in granite, which is unfavorable for strength and is relatively coarse-grained, or the quartz and feldspar particles in granite are relatively coarse-grained and have undergone fragmentation and recrystallization to form an aggregate, resulting in weak bonding strength. This idea is verified through an analysis of sandstone and granite, which reveals that the biotite minerals present in granite are mainly fine-grained and have a content of 6%, while the biotite minerals in sandstone are mainly microscopic and have a content of 11%.

A comparison of the relative specific surface areas of these two stones shows that the relative specific surface area of sandstone is smaller. However, granite has a greater number of hard mineral components and fewer soft mineral components, which should result in a smaller relative specific surface area for granite, leading to the focus shifting to the size of mineral particles. Further analysis of the relationship between the particle content of the main minerals and the relative specific surface area of the rock reveals a clear negative correlation, as shown in Fig. 7.

Figs. 6 and 7 show that the main minerals in the rock are feldspar and quartz, which are hard mineral components that have a significant impact on the breakability of the rock. For most rocks, the content of hard mineral components is inversely proportional to the specific surface area of the aggregate, but there are exceptions. The granite used in this test does not show a clear correlation between the total content of hard mineral components and the rock's breakability. Compared with sandstone, although granite has more hard mineral components and fewer soft mineral components, the relative specific surface area of the broken aggregate is larger than that of sandstone. This finding indicates that the total content of hard and soft mineral components in the rock does not always directly dominate. However, the particle content of the main minerals is well correlated with the rock's breakability to some extent.

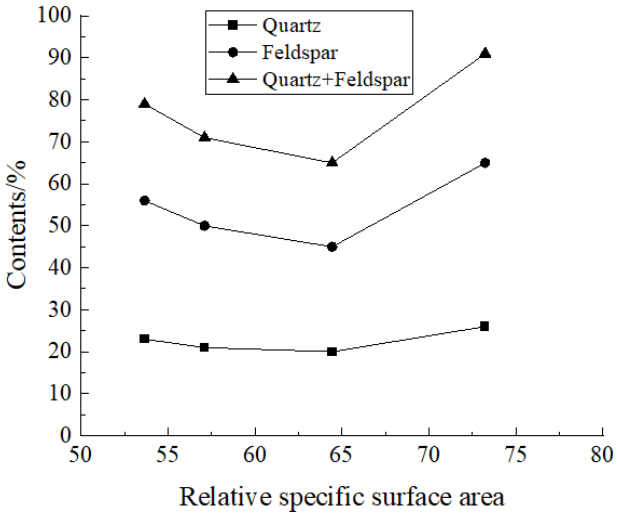

Fig. 6 Influence of Main Mineral Content on the Relative Specific Surface Area of Aggregate

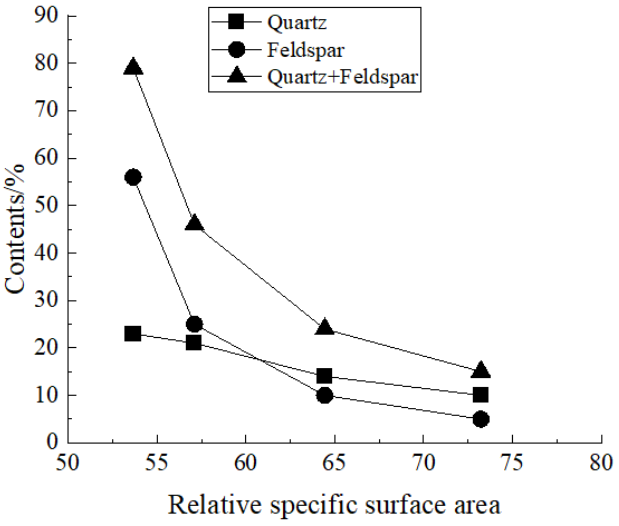

Fig. 7 Influence of Main Mineral Microparticle Content on the Relative Specific Surface Area of Aggregate

4.1.2 Influence of Mineral Particles on Rock Breakability

Comparative analysis found that the mineral particles in the four types of rocks mainly present as microscopic and fine-grained structures, with a proportion of more than 80%. Some stones contain medium-grained and coarse-grained structures, but their content is low, with less than 20%. Therefore, the influence of microscopic and fine-grained content on rock breakability became the main focus, as shown in Fig. 8.

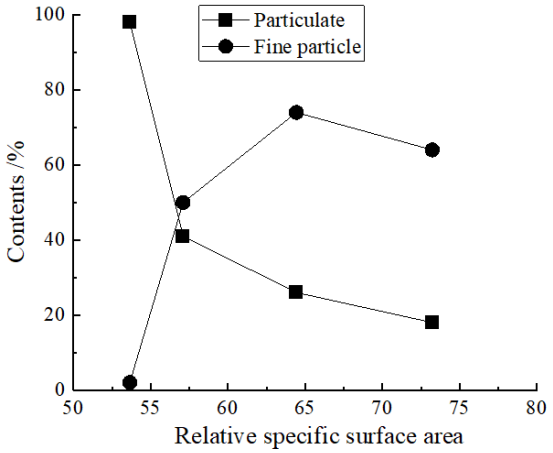

Fig. 8 Influence of Mineral Particle Size Distribution on the Relative Specific Surface Area of Aggregate

The test results indicate that a high content of microscopic mineral particles in the rock corresponds to its smaller relative specific surface area, meaning that the rock is more difficult to break. This finding reveals the negative correlation between the content of microscopic mineral particles in the rock and its breakability. Conversely, a high content of fine-grained particles in the rock corresponds to its large relative specific surface area, indicating that the rock is easier to break. This condition occurs because the increase in fine-grained content leads to a decrease in microscopic content, thus reflecting the above conclusion from another perspective. Analysis shows that granite has only 18% medium-grained mineral content, while tuff contains 7% medium-grained content and 2% coarse-grained content. The results indicate that the relative specific surface area of tuff is smaller, which clearly shows that the 2% coarse-grained content does not significantly affect the breakability of the rock.

In contrast, the medium-grained content has a greater impact. At the same time, considering that the medium-grained and coarse-grained mineral content in the rock does not exceed 20%, their impact on the breakability of the rock is relatively small. As a complex combination of physical and chemical processes, rocks have hard mineral components as a framework and soft mineral components as a binding material, encapsulating it to form a whole. Small particles of the framework correspond to a large surface area per unit volume, thus requiring more binding material. The framework particles are more compact, while larger particles require less binding material, resulting in less concentrated bonding. For rocks, in the case of the same content of binding material, larger particles are more likely to lead to excessive binding material, which forms weak aggregates that are relatively concentrated, making the rock easier to break during the fragmentation process, specifically manifesting as a larger relative specific surface area.

In summary, factors affecting the breakability of rocks include not only the mineral composition and its content but also the particle size distribution of the minerals. The total content of hard mineral components does not always directly dominate; it may be influenced by other factors, making the dominant factors more complex.

4.2 Concrete Mechanical Properties Test

4.2.1 Raw Material

The main properties of the aggregate are listed in Table 3, and the relationship between the relative specific surface area of the rock after crushing and the aggregate properties is plotted in Fig. 9.

Table 3. Main Physical Properties of Artificial Aggregate

Serial number	Fineness modulus		Stone powder content (%)		Apparent density of sand (kg/m^3)	Crushing value index of stone (%)
	Original	Before processing	Original	Before processing		
H-GL	2.3	2.7	30	13	2640	19.7
N-GL	2.5	2.7	21	13	2670	11.2
SC-GL	2.4	2.7	26	13	2650	16.4
SH-GL	2.6	2.7	15	13	2710	5.3

The test results indicate that the relative specific surface area of the aggregate is positively correlated with the content of stone powder and the crushing index of the artificial sand and negatively correlated with the fineness modulus and apparent density of the artificial sand. In other words, a large relative specific surface area corresponds to the rock's decreased ability to resist external forces, thus being easily damaged during the crushing process when subjected to pressure, impact, friction, and other actions. This condition occurs because the aggregate of soft mineral particles is more susceptible to destruction than the structure formed by binding soft particles with hard mineral particles. Therefore, a large relative specific surface area of the aggregate corresponds to a great proportion and particle size of the soft particle aggregate, leading to the generation of more stone powder, a smaller fineness modulus of the sand, and a more extensive crushing index. The internal compactness of the soft minerals is less than that of the hard minerals, so their density is smaller, resulting in a smaller apparent density of the aggregate. Conversely, a small specific surface area corresponds to the rock's increased ability to resist external forces. During the crushing process, the proportion of hard minerals is greater, and the particle size is smaller. The soft mineral particles are more dispersed around the hard minerals, forming a more stable structure bound with the hard minerals, making it difficult for the soft minerals to form weak aggregates. This condition leads to a decrease in weak aggregates, resulting in smaller crushing indices and stone powder contents, a larger fineness modulus of the sand, and a larger apparent density of the aggregate.

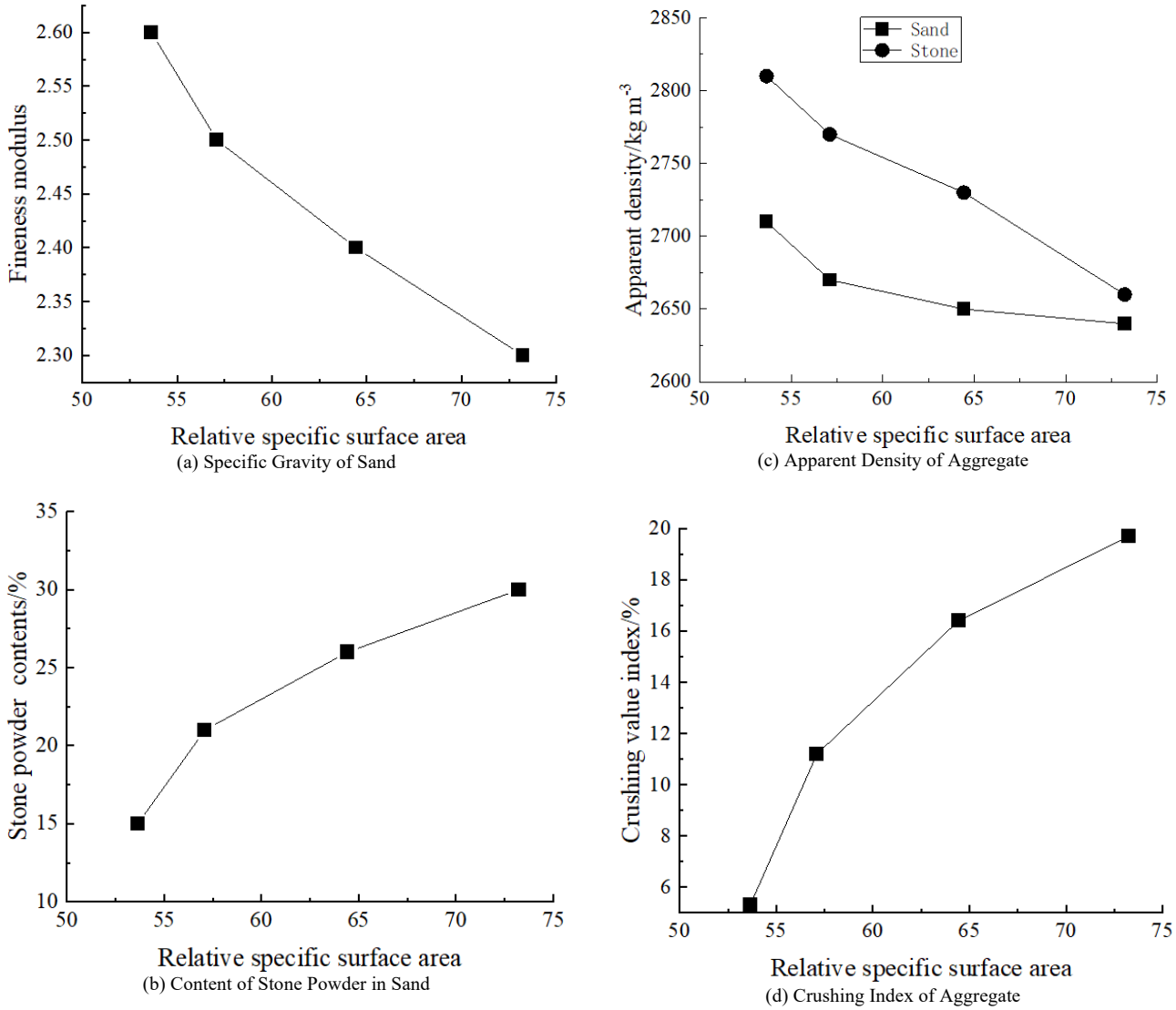

(a) Specific Gravity of Sand

(c) Apparent Density of Aggregate

(b) Content of Stone Powder in Sand

(d) Crushing Index of Aggregate

Fig. 9 Relationship Between Specific Surface Area and Aggregate Properties

Table 4. Main Parameters of Concrete Mix Proportion

Serial number	Strength grade	W/C	Amount of material per square (kg/m^3)					
			Water	Cement	Fly ash	Sand	Coarse aggregate (mm)	
							5–20	20–40
H-P1	C30	0.36	125	278	69	617	631	631
N-P1		0.41	126	246	61	655	660	660
SC-P1		0.39	125	256	64	650	650	650
SH-P1		0.43	126	234	59	670	678	678
H-P2	C40	0.28	128	366	91	546	612	612
N-P2		0.32	129	252	63	612	675	675
SC-P2		0.30	128	341	85	578	633	633
SH-P2		0.34	129	304	76	603	667	667

4.2.2 Mix Proportion

The main parameters of the concrete mix proportion for different aggregates are listed in Table 4. The adjusted artificial sand is used in the mix proportion, with the fineness modulus and stone powder content kept consistent. The aggregates are all measured in a saturated surface dry state, and the sand ratio is calculated based on volume. The gradation of the coarse aggregate for each mix proportion is medium stone: small stone = 50:50.

4.2.3 Compressive Strength and Static Compressive Elastic Modulus

The test results for compressive strength and static compressive elastic modulus are presented in Table 5. The relationship curves between the aggregate's relative specific surface area and the concrete's water-to-binder ratio and between the aggregate's relative specific surface area and the concrete's elastic modulus are plotted and presented in Fig. 10. Fig. 10a shows that for C30 and C40 concrete prepared with different aggregates within the same strength grade, as the aggregate's relative specific surface area increases, the concrete's water-to-binder ratio continuously decreases, showing a linear relationship. This result occurs because a decrease in the water-to-binder ratio means an increase in the cementitious material used in the concrete mix. Such a condition is because the concrete exhibits different failure modes under the same compressive load. For concrete with harder aggregates, the interface between

the cement paste and the aggregate is the first weak point to crack, followed by the appearance and propagation of cracks at multiple weak points until the concrete surface is perforated and the failure occurs. For concrete with softer aggregates, the weak points are more likely to appear within the coarse aggregates. Fig. 10b shows that within the same strength grade, as the aggregate's relative specific surface area increases, the concrete's elastic modulus decreases, showing a linear relationship. In this test, the air and water content of the concrete with the same strength grade is approximately the same, meaning the volume of cement paste and aggregate remains constant. For concrete with harder aggregates, the deformation of the aggregate itself is smaller, and the volume ratio of the aggregate in this mix proportion is larger, further restricting the deformation of the concrete. This condition ultimately leads to a higher static compressive elastic modulus for the concrete[22]. For C30 concrete, as the water-to-binder ratio increases from 0.36 to 0.43, the water-to-binder ratio increases by 19.4%, and the static compressive elastic modulus increases by 22.5%. For C40 concrete, as the water-to-binder ratio increases from 0.28 to 0.34 (a 21.4% increase), the static compressive elastic modulus increases by 25.0%.

Table 5. Concrete Performance Test Results

Serial number	Strength grade	W/C	Compressive strength (MPa)	Axial compressive strength (MPa)	Static compressive elastic modulus (GPa)
H-P1	C30	0.36	37.6	26.4	22.7
N-P1		0.41	37.9	27.2	26.1
SC-P1		0.39	38.1	27.3	24.9
SH-P1		0.43	38.4	27.6	27.8
H-P2	C40	0.28	48.9	35.2	30.8
N-P2		0.32	48.5	34.9	36.7
SC-P2		0.30	48.7	35.1	34.1
SH-P2		0.34	48.6	35.0	38.5

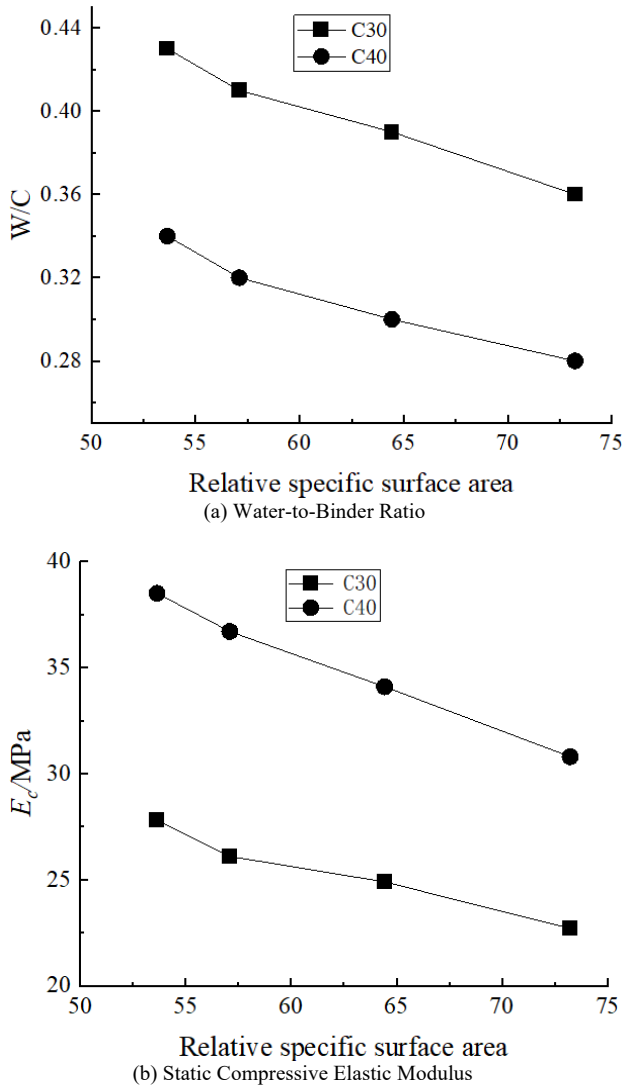

(a) Water-to-Binder Ratio

(b) Static Compressive Elastic Modulus

Fig. 10 Relationship between Relative Specific Surface Area of Aggregate and Water-to-Binder Ratio and Elastic Modulus of Concrete

5. Conclusions

To quantitatively assess the difficulty of rock fragmentation and efficiently apply the broken rock aggregate in concrete materials, a physical parameter was proposed to quickly compare the difficulty of rock fragmentation, characterizing the breakability of rocks and the processability of aggregates. The relationship between the relative specific surface area of aggregates and their main physical properties was established, and the performance impact of rock breakability on the elastic modulus of concrete was analyzed. The following conclusions could be drawn:

(1) The breakability of rocks is related to the mineral composition and content and the particle size distribution of mineral grains. For most rocks, the total content of hard mineral components plays a direct dominant role. The mineral particles of granite, tuff, diorite, and sandstone investigated in this study mainly exhibit microscopic and fine-grained structures, with a proportion of more than 80%, and the content of medium-grained and coarse-grained structures is less than 20%.

(2) The relative specific surface area of the rock is positively correlated with the content of stone powder and the crushing index of artificial sand and negatively correlated with the fineness modulus and apparent density of artificial sand.

(3) Within the same strength grade, as the aggregate's relative specific surface area increases, the concrete's water-to-binder ratio continuously decreases. Increased hardness of the aggregate corresponds to a lower required amount of cementitious material, making the concrete more economical. The relative specific surface area of the aggregate is negatively correlated with the elastic modulus of the concrete, indicating that a large relative specific surface area of the aggregate corresponds to a small elastic modulus of the concrete and a large deformation under the same load. In other words, a small relative specific surface area of the aggregate corresponds to a large elastic modulus of the concrete and small deformation.

(4) Under the condition of meeting the requirements of processing technology, the aggregates with a smaller relative specific surface area are harder, which is beneficial

to reducing the cementitious material usage but may cause more wear on the equipment and poorer deformation capacity. The aggregates with a larger relative specific surface area are softer and require more cementitious material to ensure strength. For C30 concrete, the water-to-binder ratio increases by 19.4%, and the static compressive elastic modulus increases by 22.5%; for C40 concrete, the water-to-binder ratio increases by 21.4%, and the static compressive elastic modulus increases by 25.0%.

Laboratory experiments were combined with theoretical studies to propose a convenient method for evaluating rock breakability: the relative specific surface area of aggregates. It can quickly compare the physical and mechanical properties of different rock aggregates and their impact on the elastic modulus of concrete, providing specific guidance for achieving rapid and effective rock fragmentation and resource utilization of aggregates. With the lack of examples of resource utilization of broken rock aggregates, the application of this study's findings in practical engineering will further verify the practical application effects of this study and promote the application of the findings in future studies.

References

[1] S. Hosseini, R. Poormirzaee, and M. Hajihassani, "An uncertainty hybrid model for risk assessment and prediction of blast-induced rock mass fragmentation," *Int. J. Rock Mech. Min. Sci.*, vol. 160, Dec. 2022, Art. no. 105250.

[2] J. Zou, W. Yang, T. Zhang, X. Wang, and M. Gao, "Experimental investigation on hard rock fragmentation of inserted tooth cutter using a newly designed indentation testing apparatus," *Int. J. Min. Sci. Techno.*, vol. 32, no. 3, pp. 459-470, May 2022.

[3] X. Li, K. Liu, Y. Sha, J. Yang, and R. Song, "Numerical investigation on rock fragmentation under decoupled charge blasting," *Comput. Geotech.*, vol. 157, May 2023, Art. no. 105312.

[4] Y. Luo, X. Zhu, W. Liu, Y. Zhang, H. Hu, L. He, and M. Chen, "Rock fragmentation and drilling experiment of electric impulse drilling and structural optimization of electrode bit," *Geoenergy Sci. Eng.*, vol. 227, Aug. 2023, Art. no.211896.

[5] M. Kucewicz, M. Łukasz, P. Baranowski, J. Małachowski, K. Fuławka, P. Mertuszka, and M. Szumny, "Numerical modeling of blast-induced rock fragmentation in deep mining with 3D and 2D FEM method approaches," *J. Rock. Mech. Geotech.*, to be published. Accessed: May 2024. doi: 10.1016/j.jrmge.2024.01.017. [Online]. Available: https://doi.org/10.1016/j.jrmge.2024.01.017.

[6] M. Sharma, B.S. Choudhary, A.K. Raina, M. Khandelwal, and S. Rukhiyar, "Prediction of rock fragmentation in a fiery seam of an open-pit coal mine in India," *J. Rock. Mech. Geotech.*, to be published. Accessed: April, 2024. doi: 10.1016/j.jrmge.2023.11.047. [Online]. Available: https://doi.org/10.1016/j.jrmge.2023.11.047.

[7] X. Shang, J. Zhou, F. Liu, J. Shen, and X. Liao, "A peridynamics study for the free-surface-assisted rock fragmentation caused by TBM disc cutters," *Comput. Geotech.*, vol. 158,Jun. 2023, Art. no.105380.

[8] X. Zhang, H. Jiang, H. Li, C. Gu, and L. Zhao, "Rock fragmentation using the disc tool assisted by the prefabricated kerf: Numerical modelling based on discrete element method (DEM)," *Eng. Fract. Mech.*, vol. 282, Apr. 2023, Art. no. 109159.

[9] T. Chen, and S. Xiao, "Three-dimensional numerical prediction of elastic modulus of concrete as a three-phase composite with asymptotic homogenization," *Constr. Build. Mater.*, vol. 348, Sep. 2022, Art. no. 128640.

[10] C. Liang, *et al*, "Enhancing the elastic modulus of concrete prepared with recycled coarse aggregates of different quality by chemical modifications," *Constr. Build. Mater.*, vol. 360, Dec. 2022, Art. no. 129590.

[11] B. He, J. Wang, Y. Zhang, S. Yan, and T. Chen, "Microscopic failure of yellow sandstone with different-sized grains and mineral composition," *J. Cent. South Univ.*, vol. 30, no. 6, pp. 2035-2047, Jul. 2023.

[12] G.B. Crosta, G. Dattola, C. Lanfranconi, F.V. De Blasio, M. Malusa, and D. Bertolo, "Rockfalls, fragmentation, and dust clouds: analysis of the 2017 Pousset event (Northern Italy)," *Landslides*, vol. 20, no. 12, pp. 2545-2562, Aug. 2023.

[13] A. Azadmehr, S.M.E. Jalali, and Y. Pourrahimian, "An application of rock engineering system for assessment of the rock mass fragmentation: A hybrid approach and case study," *Rock Mech. Rock Eng.*, vol. 52, no. 11, pp. 4403-4419, Jun. 2019.

[14] T. Bamford, K. Esmaeili, and A.P. Schoellig, "A real-time analysis of post-blast rock fragmentation using UAV technology," *Int. J. Min. Reclam. Env.*, vol. 31, no. 6, pp. 439-456, Jun. 2017.

[15] M. Räisänen, "Relationships between texture and mechanical properties of hybrid rocks from the Jaala-Iitti complex, southeastern Finland," *Eng. Geol.*, vol. 74, no. 3-4, pp. 197-211, Aug. 2004.

[16] Y. Wang and F. Tonon, "Discrete element modeling of rock fragmentation upon impact in rock fall analysis," *Rock Mech. Rock Eng.*, vol. 44, no. 1, pp. 23-35, Jan. 2011.

[17] B. Elevli, I. Topal, and S. Elevli, "Multivariate statistics application in development of blast fragmentation charts for different rock formations in quarries," *Acta Montan. Slovaca*, vol. 17, no. 4, pp. 300-309, Dec. 2012.

[18] A. Tosun, "A new method for determining muckpile fragmentation formed by blasting," *J. South. Afr. Inst. Min. Metall.*, vol. 122, no. 11, pp. 665-672, Nov. 2022.

[19] A. Hatheway, "The complete isrm suggested methods for rock characterization, testing and monitoring; 1974-2006," *Environ. Eng. Geosci*., vol. 15,no.1,pp. 47-48, Feb. 2009.

[20] A.V. Abioye, "Relationship of brittleness and fragmentation in brittle compression," *Eng. Geol.*, vol. 221, pp. 82-90, Apr. 2017.

[21] Y. Ni, Z. Wang, S. Li, J. Wang, and C. Feng, "Numerical study on the dynamic fragmentation of rock under cyclic blasting and different in-situ stresses," *Comput. and Geotech.,* vol. 172, Aug. 2024, Art. no.106404.

[22] F.P. Zhou, F.D. Lydon, and B.I.G. Barr, "Effect of coarse aggregate on elastic modulus and compressive strength of high performance concrete," *Cem. Concr. Res.*, vol. 25, no. 1, pp. 177-186, Jan. 1995.